C. R. Mecanique 346 (2018) 571–580

Contents lists available at ScienceDirect

Comptes Rendus Mecanique

www.sciencedirect.com

Model reduction, data-based and advanced discretization in computational mechanics

Conserving and decaying energy for finite-strain three-dimensional solids with rotational degrees of freedom in nonlinear dynamics

Conservation et dissipation d'énergie dans les solides tridimensionnels en grandes transformations avec des degrés de liberté rotationnels en dynamique non linéaire

Abir Boujelben [a], Adnan Ibrahimbegovic [b]

[a] *Sorbonne Universités, Université de technologie de Compiègne, Laboratoire Roberval de mécanique, Centre de recherches de Royallieu, CS 60319, 60200 Compiègne cedex, France*
[b] *Sorbonne Universités, Université de technologie de Compiègne, Laboratoire Roberval de mécanique, Chair of Computational Mechanics, Centre de recherches de Royallieu, CS 60319, 60200 Compiègne cedex, France*

ARTICLE INFO

Article history:
Received 4 May 2017
Accepted 23 January 2018
Available online 9 May 2018

Keywords:
3D solids
Nonlinear dynamics
Large displacements and rotations
Conserving/decaying algorithms

Mots-clés :
Solide 3D
Dynamique non linéaire
Grandes transformations
Algorithme de conservation/dissipation

ABSTRACT

In this work, we design a time-stepping scheme, which can ensure either conservation of energy or dissipation of energy of high (unresolved) modes for nonlinear dynamic analysis. The latter is needed to improve the performance in stress computation and long-term numerical stability. Finite element implementation details are given for finite-strain three-dimensional solid model with independent rotational degrees of freedom. The addition of a rotation field requires a particular choice of large strain measures, allowing one to separate large rotation and large displacement. Several numerical simulations illustrate a very satisfying performance of the proposed time-stepping scheme.

RÉSUMÉ

Dans cet article, nous développons un schéma implicite d'intégration temporelle capable d'assurer, soit la conservation de l'énergie, soit la dissipation de l'énergie d'un système dynamique non linéaire. Ce dernier est particulièrement intéressant pour améliorer la stabilité numérique pour le calcul sur un grand intervalle du temps. L'implémentation de la méthode des éléments finis est présentée en détail pour un modèle de solide tridimensionnel en grandes transformations qui fait intervenir des degrés de liberté de rotation indépendants. La prise en compte de la rotation implique un choix judicieux de la mesure des grandes déformations pour séparer les grands déplacements des grandes

E-mail addresses: abir.boujelben@utc.fr (A. Boujelben), adnan.ibrahimbegovic@utc.fr (A. Ibrahimbegovic).

https://doi.org/10.1016/j.crme.2018.04.006

rotations. La performance du schéma proposé est illustrée à travers de nombreux exemples de simulations.

Version française abrégée

L'analyse dynamique non linéaire s'effectue généralement par des schémas d'intégration temporelle, en privilégiant les schémas implicites tels que celui de Newmark, car ils n'imposent pas de restrictions sévères pour le choix du pas de temps. Cependant, dans le cas des systèmes raides où la réponse est dominée par une grande différence des modes à basse et à haute fréquences, ces schémas ne sont pas suffisants pour garantir la stabilité du calcul numérique. Pour surmonter ce problème, nous développons un schéma d'intégration qui garantit la conservation de l'énergie à chaque pas de temps et qui permet, en cas de besoin, de forcer la dissipation numérique de la contribution des hautes fréquences.

Dans ce travail, nous nous intéressons plus particulièrement à l'implémentation de la méthode des éléments finis pour le schéma proposé de modèle de solide tridimensionnel en grandes transformations qui fait intervenir des degrés de liberté rotationnels indépendants. La prise en compte des rotations implique un choix spécifique de la mesure de la déformation : la déformation de Biot. Les approximations discrètes des champs de déplacement et de rotation sont obtenues par une interpolation linéaire standard. Afin d'homogénéiser l'approximation des mesures de déformation, on fait appel à la méthode des modes incompatibles, permettant d'augmenter l'ordre de l'approximation du champ de déplacement par l'addition d'un champ de déplacement amélioré (quadratique).

Le problème est présenté sous une formulation variationnelle régularisée en grandes déformations, avec une forme quadratique simple du terme d'inertie – voir l'Éq. (3). Ce dernier est exprimé en termes de déplacements, tandis que le champ de rotation contribue uniquement aux mesures de la déformation. Ceci implique la présence d'un bloc de termes nuls associés aux degrés de liberté de rotation dans la matrice masse, provoquant des modes en fréquences infinies. Pour contrôler l'effet indésirable de ces modes, nous proposons d'abord d'introduire une forme régularisée des termes d'inertie associés aux degrés de liberté de rotation, afin d'éviter la présence des fréquences infinies. Ensuite, nous exploitons le schéma de conservation d'énergie afin d'assurer la stabilité du calcul, même en cas de domination de modes à hautes fréquences, qui apparaissent comme le résultat de la régularisation.

Le schéma proposé est basé sur le schéma de point milieu, en y apportant quelques modifications afin de satisfaire le caractère conservatif. D'une part, ces modifications concernent une expression alternative de la relation de comportement en $t_{n+\frac{1}{2}}$ sous forme algorithmique, de telle sorte que le terme de déformation dans la formulation variationnelle corresponde à l'incrément de l'énergie potentielle – voir les Éqs. (12) et (13). D'autre part, une approximation spécifique du vecteur de vitesse linéaire permet d'égaliser le terme d'inertie et l'incrément de l'énergie cinétique – voir les Éqs. (10) et (11). En supposant que les efforts extérieurs sont conservatifs, la conservation d'énergie est bien assurée. Un autre enjeu s'impose lors de la construction du schéma d'intégration : c'est l'approximation du champ de rotation, qui est extrêmement non linéaire. Dans une démarche de simplification, on retient une approximation linéaire.

Une autre alternative proposée pour contrôler les problèmes d'instabilité causés par des systèmes d'équations raides consiste à introduire une dissipation numérique des hautes fréquences à chaque pas de temps. L'originalité de ce schéma réside dans l'addition des termes dissipatifs – voir les Éqs. (18) et (20) – sans toucher à l'algorithme défini dans le cas de la conservation d'énergie, de manière à ce que les deux schémas puissent partager le même espace de stockage pour les variables internes. Autrement dit, les modifications concernent seulement l'actualisation du vecteur de vitesse et la relation algorithmique du comportement.

En conclusion, la conservation ou la dissipation de l'énergie totale est une propriété importante des schémas d'intégration temporelle, particulièrement pour des calculs sur un grand intervalle de temps, où l'on souhaite atténuer l'effet indésirable des hautes fréquences sur le déclenchement d'instabilités, sans oublier la contribution de la régularisation de masse dans le cas du solide 3D avec des degrés de liberté de rotation. D'ailleurs, ce modèle se révèle favorable pour l'analyse de structures combinées d'éléments solides et d'éléments structures, d'autant plus que plusieurs travaux antérieurs ont été réalisés à propos de la conservation d'énergie d'éléments poutres.

1. Introduction

The dynamic analysis of geometrically nonlinear problems dominated by high-frequency modes is extremely difficult to solve by using standard implicit time-stepping schemes, such as Newmark's method. To resolve this important issue, a very active research have been elaborated on conserving or/and decaying energy time-stepping schemes for nonlinear dynamics of rods [1–3] and shell-like structures [4,5] undergoing large overall motion. The main motivation of these approaches is to ensure the satisfying computational performance in the case of stiff problems, mainly for long-term response.

In this paper, we are interested in the regularized variational formulation for the nonlinear dynamics of three-dimensional solid with independent rotational degrees of freedom. The formulation is set in a fixed frame, featuring a

simple quadratic form of the kinetic energy. The latter is expressed only in terms of the displacement field, since the rotation field is involved just to compute the large strain measures. This leads to the presence of zero terms in the mass matrix associated with the rotational degrees of freedom requiring infinite frequencies and disrupting the computation stability. Therefore, we seek to construct an energy conserving time-stepping scheme to overcome the deficiency of (unresolved) high-frequency participation. This scheme is based on the mid-point approximation. The pertinent modifications that are needed to enforce the energy conservation are algorithmic constitutive equations and appropriate choice of rotation and velocity updates.

In seeking to improve the robustness of the scheme stability performance, we propose to redesign the energy conserving scheme by introducing desirable properties of controllable dissipation in higher modes. The main idea is to add regularized terms to algorithmic stress resultants and velocity updates, and to assure an artificial energy dissipation of the high-frequency modes.

The outline of the paper is as follows. In the next section, we present the regularized variational formulation in dynamics of the proposed enhanced 3D solid undergoing large overall motion. In Section 3, we examine in detail the formulation and the implementation of a time-stepping energy conserving/decaying schemes for the proposed model. A set of illustrative numerical simulations is presented in Section 4, showing an excellent performance of the proposed scheme. Some concluding remarks are given in Section 5.

2. Variational formulations and finite element implementation

2.1. Hamilton principle in dynamics

We consider a three-dimensional solid model with rotational degrees of freedom undergoing overall large motion in geometrically nonlinear dynamic problems. The Biot strain $\mathbf{H}$ is chosen to define strain measures: $\mathbf{H} = \mathbf{R}^{\mathsf{T}}(\mathbf{I}+\mathbf{D}) - \mathbf{I}$. The latter introduces explicitly the rotation tensor $\mathbf{R}$ defined through the polar decomposition of deformation gradient [6]. In order to improve the performance of the discrete approximation, the enhanced displacement gradient is defined through the displacement gradient $\mathbf{D}$, given as a sum of the standard displacement gradient $\nabla\mathbf{u}$ and of an enhanced displacement gradient $\mathbf{d}$ provided by the method of incompatible modes.

The equations of motion are obtained by appealing to the classical Hamilton principle [7]:

$$\begin{aligned}
&(i)\quad \mathbf{T}(\mathbf{u}) = \int_{\mathbf{V}} \frac{1}{2}\,\dot{\mathbf{u}}\cdot\rho\,\dot{\mathbf{u}}\,\mathrm{d}\mathbf{V}\\
&(ii)\quad \Pi(\mathbf{u},\mathbf{R},\mathbf{d}) = \int_{\mathbf{V}} \{\frac{1}{2}\,\mathrm{symm}[\mathbf{R}^{\mathsf{T}}(\mathbf{I}+\mathbf{D})-\mathbf{I}]\cdot\mathbf{C}\,\mathrm{symm}[\mathbf{R}^{\mathsf{T}}(\mathbf{I}+\mathbf{D})-\mathbf{I}]\\
&\quad + \frac{1}{2}\,\mathrm{skew}[\mathbf{R}^{\mathsf{T}}(\mathbf{I}+\mathbf{D})-\mathbf{I}]\cdot\gamma\,\mathrm{skew}[\mathbf{R}^{\mathsf{T}}(\mathbf{I}+\mathbf{D})-\mathbf{I}] - \mathbf{P}\cdot\mathbf{d}\}\,\mathrm{d}\mathbf{V} - \int_{\mathbf{V}} \mathbf{u}\cdot\mathbf{f}\,\mathrm{d}\mathbf{V}
\end{aligned} \tag{1}$$

where $\mathbf{P}$ is the first Piola–Kirchoff stress tensor, conjugated to the enhanced displacement gradient $\mathbf{d}$, whereas γ is the regularization parameter. We emphasize that the kinetic energy is expressed only in terms of displacement field, which implies the presence of zero masses associated with the rotation degrees of freedom. This leads to infinite frequencies and the extreme stiff problem with all the difficulties that it will impose. These difficulties are more pronounced in the case of a 3D solid element capable of representing more vibration modes compared to structure elements. For that reason, in addition of a energy conserving time-stepping scheme, it is particularly necessary to add the mass matrix contribution of the angular acceleration in order to reduce the influence of infinite frequencies. This contribution is presented in the form of a regularized expression for kinetic energy, equal to a similar quadratic form but multiplied by a coefficient α that varies from 0 to 1. Therefore, one can attenuate the high-frequency content in the structural motion simply by choosing larger values for the mass regularization parameter α.

For computational efficiency, we further switch to the compact form matrix notation, detailed in Appendix A. We denote by $\boldsymbol{\Gamma}$ and $\mathbf{L}$ the stress resultants, energy conjugates to the symmetric part $\mathbf{e}$ and the skew-symmetric part $\boldsymbol{\omega}$ of the strain measures written in a matrix form, respectively,

$$\boldsymbol{\Gamma}(\mathbf{u},\mathbf{R},\mathbf{d}) := \mathbf{C}\,\mathbf{e}(\mathbf{u},\mathbf{R},\mathbf{d});\ \ \mathbf{L}(\mathbf{u},\mathbf{R},\mathbf{d}) := \gamma\,\boldsymbol{\omega}(\mathbf{u},\mathbf{R},\mathbf{d}) \tag{2}$$

Then, the corresponding variational equations can be written as

$$\begin{aligned}
\begin{Bmatrix}\delta\mathbf{u}\\ \delta\mathbf{w}\end{Bmatrix}\cdot\mathbf{r}(\mathbf{u},\mathbf{R},\mathbf{d},\mathbf{p}) &:= \int_{\mathbf{V}}\delta\mathbf{u}\cdot\rho\ddot{\mathbf{u}}\,\mathrm{d}\mathbf{V}+\int_{\mathbf{V}}\{\delta\mathbf{e}\cdot\mathbf{C}\mathbf{e}(\mathbf{u},\mathbf{R},\mathbf{d})+\delta\boldsymbol{\omega}\cdot\gamma\boldsymbol{\omega}(\mathbf{u},\mathbf{R},\mathbf{d})\}-\int_{\mathbf{V}}\delta\mathbf{u}.\mathbf{f}\,\mathrm{d}\mathbf{V}=0\\
\delta\mathbf{d}\cdot\mathbf{h}(\mathbf{u},\mathbf{R},\mathbf{d},\mathbf{p}) &:= \int_{\mathbf{V}}\{\delta\mathbf{d}\cdot\boldsymbol{\Lambda}^{\mathsf{T}}(\mathbf{R})\mathbf{C}\mathbf{e}(\mathbf{u},\mathbf{R},\mathbf{d})+\delta\mathbf{d}\cdot\boldsymbol{\Xi}^{\mathsf{T}}(\mathbf{R})\gamma\boldsymbol{\omega}(\mathbf{u},\mathbf{R},\mathbf{d})-\delta\mathbf{d}^{\mathsf{T}}\mathbf{p}\}\,\mathrm{d}\mathbf{V}=0\\
\delta\mathbf{p}\cdot\mathbf{g}(\mathbf{u},\mathbf{R},\mathbf{d},\mathbf{p}) &:= \int_{\mathbf{V}}\{\delta\mathbf{p}^{\mathsf{T}}\mathbf{d}\}\,\mathrm{d}\mathbf{V}=0
\end{aligned}\tag{3}$$

2.2. Discrete approximation

The discrete approximations for the standard displacement field and the rotation field are constructed according to the standard isoparametric interpolation for an 8-node 3D solid element with

$$\mathbf{u}(\underline{\mathbf{x}},t)=\sum_{I=1}^{8}N_I(\underline{\mathbf{x}})\mathbf{u}_I(t)\equiv\mathbf{N}\mathbf{u}^{\mathrm{e}}(t);\ \mathbf{w}(\underline{\mathbf{x}},t)=\sum_{I=1}^{8}N_I(\underline{\mathbf{x}})\mathbf{w}_I(t)\equiv\mathbf{N}\mathbf{w}^{\mathrm{e}}(t)\tag{4}$$

where N_I are the standard shape functions, while $\mathbf{u}_I$ and $\mathbf{w}_I$ are the corresponding nodal values.

The enhanced displacement gradient are approximated by using derivatives of the incompatible displacement $\boldsymbol{\alpha}$

$$\mathbf{d}(\underline{\mathbf{x}},t)=\sum_{J=1}^{N_{\mathrm{im}}}\hat{\mathbf{G}}_J(\underline{\mathbf{x}})\boldsymbol{\alpha}_J(t)\equiv\hat{\mathbf{G}}(\underline{\mathbf{x}})\boldsymbol{\alpha}^{\mathrm{e}}(t),\ \hat{\mathbf{G}}=\left[\hat{\mathbf{G}}_1,\hat{\mathbf{G}}_2,\hat{\mathbf{G}}_3\right],\quad \hat{\mathbf{G}}_I=\begin{bmatrix}\frac{\partial M_I}{\partial x_1}\mathbf{I}_3\\ \frac{\partial M_I}{\partial x_2}\mathbf{I}_3\\ \frac{\partial M_I}{\partial x_3}\mathbf{I}_3\end{bmatrix}\tag{5}$$

where $M_1=(1-\xi^2)$, $M_2=(1-\eta^2)$ and $M_3=(1-\zeta^2)$ are chosen as quadratic polynomials. In order to ensure the convergence of incompatible mode method in the spirit of patch test [8], we impose that $\int_{\mathbf{V}}\hat{\mathbf{G}}\,\mathrm{d}\mathbf{V}=0$, eliminating $\mathbf{P}$ from the variational equations.

3. Energy conserving/decaying schemes

3.1. Energy conserving scheme

In this section, we seek to design a time-stepping scheme that ensures energy conservation. At a typical time t_n, the values of $\mathbf{u}_n$ and $\mathbf{R}_n$ are known. The corresponding values at time t_{n+1} are computed in each step independently for single-step schemes: for the displacement vector, we have sample additive updates

$$\mathbf{u}_{n+1}^{(i+1)}=\mathbf{u}_{n+1}^{(i)}+\Delta\mathbf{u}_{n+1}^{(i)}\tag{6}$$

where $\Delta\mathbf{u}_{n+1}^{(i)}$ is the incremental displacement at each iteration (i). The rotation update is somewhat more involved in that we have to choose between various possibilities of parameters for rotation representation [9]. In geometrically exact beam theory, Simo and Tarnow proposed to use the material rotation vector with Cayley transform mapping in order to assure rotation updates [10]. However, we opted for a quaternion representation that reduces the rotation tensor to four parameters (see, e.g., [11]), providing a more efficient computational procedure by replacing the matrix multiplication by the quaternion algebra. Then, the rotational updates can be written by using the axial vector of incremental rotation $\Delta\mathbf{w}_{n+1}^{(i)}$ as

$$\begin{aligned}
&\mathbf{R}_{n+1}^{(i+1)}=(2q_{(n+1)0}^{(i+1)2}-1)\mathbf{I}_3+2q_{0(n+1)}^{(i+1)}[\mathbf{q}_{n+1}^{(i+1)}\times\mathbf{I}_3]+2\mathbf{q}_{n+1}^{(i+1)}\otimes\mathbf{q}_{n+1}^{(i+1)}\\
&q_{0(n+1)}^{(i+1)}=q_{w0(n+1)}^{(i)}\,q_{0(n+1)}^{(i)}-\mathbf{q}_{w(n+1)}^{(i)}.\mathbf{q}_{n+1}^{(i)};\ \mathbf{q}_{n+1}^{(i+1)}=q_{w0(n+1)}^{(i)}\mathbf{q}_{n+1}^{(i)}+q_{0(n+1)}^{(i)}.\mathbf{q}_{w(n+1)}^{(i)}+\mathbf{q}_{w(n+1)}^{(i)}\times\mathbf{q}_{n+1}^{(i)}\\
&\{q_{w0(n+1)}^{(i)},\mathbf{q}_{w(n+1)}^{(i)}\}=\{\cos(\frac{\Delta w_{n+1}^{(i)}}{2}),\frac{sin(\frac{\Delta w_{n+1}^{(i)}}{2})}{\Delta w_{n+1}^{(i)}}\mathbf{w}_{n+1}^{(i)}\};\ \Delta w_{n+1}^{(i)}=(\Delta\mathbf{w}_{n+1}^{(i)}.\Delta\mathbf{w}_{n+1}^{(i)})^{\frac{1}{2}}
\end{aligned}\tag{7}$$

We assume that the displacement and rotation field are expressed at $t_{n+\frac{1}{2}}$ by a linear approximation. This plays a crucial role in the design of the proposed scheme namely for the rotation field, which is highly nonlinear.

$$\mathbf{u}_{n+\frac{1}{2}}=\frac{1}{2}(\mathbf{u}_{n+1}+\mathbf{u}_n);\ \mathbf{R}_{n+\frac{1}{2}}=\frac{1}{2}(\mathbf{R}_{n+1}+\mathbf{R}_n)\tag{8}$$

The time discretization of the weak form of the equations of motion is established, using the mid-point rule approximation.

$$
\begin{aligned}
&(i) \quad \int_{\vartheta} \delta\mathbf{u}\cdot\rho\ddot{\mathbf{u}}_{n+\frac{1}{2}}\,\mathrm{d}\vartheta + \int_{\vartheta}\{\delta\mathbf{e}(\mathbf{u}_{n+\frac{1}{2}},\mathbf{R}_{n+\frac{1}{2}},\mathbf{d}_{n+\frac{1}{2}})\cdot\boldsymbol{\Gamma}_{n+\frac{1}{2}} + \delta\boldsymbol{\omega}(\mathbf{u}_{n+\frac{1}{2}},\mathbf{R}_{n+\frac{1}{2}},\mathbf{d}_{n+\frac{1}{2}})\cdot\mathbf{L}_{n+\frac{1}{2}}\} \\
&-\int_{\vartheta}\delta\mathbf{u}.\mathbf{f}_{n+\frac{1}{2}}\,\mathrm{d}\vartheta = 0 \\
&(ii) \quad \int_{\vartheta}\{\delta\mathbf{d}\cdot\boldsymbol{\Lambda}^{\mathsf{T}}(\mathbf{R}_{n+\frac{1}{2}})\boldsymbol{\Gamma}_{n+\frac{1}{2}} + \delta\mathbf{d}\cdot\boldsymbol{\Xi}^{\mathsf{T}}(\mathbf{R}_{n+\frac{1}{2}})\mathbf{L}_{n+\frac{1}{2}}\}\mathrm{d}\vartheta = 0
\end{aligned}
\tag{9}
$$

where the linear acceleration $\ddot{\mathbf{u}}_{n+\frac{1}{2}}$ is computed using the mid-point approximation as

$$
\ddot{\mathbf{u}}_{n+\frac{1}{2}} = \frac{\dot{\mathbf{u}}_{n+1}-\dot{\mathbf{u}}_n}{\Delta t};\ \dot{\mathbf{u}}_{n+1} = -\dot{\mathbf{u}}_n + \frac{2}{\Delta t}\mathbf{u}_{n+1} \tag{10}
$$

By using the result in (10), the first term in $(9)_{(1)}$ can be written as the corresponding increment of kinetic energy

$$
\Delta\mathbf{T} = \int_{\mathbf{V}}\delta\mathbf{u}\cdot\rho\ddot{\mathbf{u}}_{n+\frac{1}{2}}\,\mathrm{d}\mathbf{V} = \int_{\mathbf{V}}\frac{\Delta t}{2}(\dot{\mathbf{u}}_{n+1}+\dot{\mathbf{u}}_n)\cdot\rho\frac{1}{\Delta t}(\dot{\mathbf{u}}_{n+1}-\dot{\mathbf{u}}_n)\,\mathrm{d}\mathbf{V} = \mathbf{T}_{n+1}-\mathbf{T}_n \tag{11}
$$

To ensure that the rest of $(9)_{(1)}$ gives the increment of internal energy, the stress resultants at $t_{n+\frac{1}{2}}$ must be computed with a particular choice of algorithmic constitutive equations

$$
\boldsymbol{\Gamma}^{\mathrm{alg}}_{n+\frac{1}{2}} = \frac{1}{2}\mathbf{C}\ (\mathbf{e}_{n+1}+\mathbf{e}_n);\ \ \mathbf{L}^{\mathrm{alg}}_{n+\frac{1}{2}} = \frac{1}{2}\gamma\ (\boldsymbol{\omega}_{n+1}+\boldsymbol{\omega}_n) \tag{12}
$$

which leads to

$$
\begin{aligned}
\Delta\Pi_{\mathrm{int}} &= \int_{\mathbf{V}}\{\delta\mathbf{e}(\mathbf{u}_{n+\frac{1}{2}},\mathbf{R}_{n+\frac{1}{2}},\mathbf{d}_{n+\frac{1}{2}})\cdot\boldsymbol{\Gamma}^{\mathrm{alg}}_{n+\frac{1}{2}} + \delta\boldsymbol{\omega}(\mathbf{u}_{n+\frac{1}{2}},\mathbf{R}_{n+\frac{1}{2}},\mathbf{d}_{n+\frac{1}{2}})\cdot\mathbf{L}^{\mathrm{alg}}_{n+\frac{1}{2}}\}\,\mathrm{d}\mathbf{V} \\
&= \int_{\mathbf{V}}\{\frac{1}{2}(\mathbf{e}_{n+1}-\mathbf{e}_n)\cdot\mathbf{C}(\mathbf{e}_{n+1}+\mathbf{e}_n) + \frac{1}{2}(\boldsymbol{\omega}_{n+1}-\boldsymbol{\omega}_n)\cdot\gamma(\boldsymbol{\omega}_{n+1}+\boldsymbol{\omega}_n)\}\,\mathrm{d}\mathbf{V} \\
&= \Pi_{\mathrm{int}}|_{n+1} - \Pi_{\mathrm{int}}|_n
\end{aligned}
\tag{13}
$$

Without loss of generality for our purpose, we assume that the external loading is obtained from a potential, assuring that $\Delta\Pi_{\mathrm{ext}} = \Pi_{\mathrm{ext}}|_{n+1} - \Pi_{\mathrm{ext}}|_n$. Thus, with the results in (11) and (13), we get the form $(9)_{(1)}$

$$
\begin{Bmatrix}\delta\mathbf{u}\\ \delta\mathbf{w}\end{Bmatrix}\cdot\mathbf{r}(\mathbf{u}_{n+1},\mathbf{R}_{n+1},\mathbf{d}_{n+1}) = 0 \rightarrow \underbrace{\Pi_{n+1}}_{\Pi_{\mathrm{ext}}|_{n+1}+\Pi_{\mathrm{int}}|_{n+1}} + \mathbf{T}_{n+1} = \Pi_n + \mathbf{T}_n \tag{14}
$$

By using the variation of strain measures, the variational equations in (9) are rewritten as

$$
\begin{aligned}
&(i) \quad \int_{\mathbf{V}}\delta\mathbf{u}\cdot\rho\ddot{\mathbf{u}}_{n+\frac{1}{2}}\,\mathrm{d}\mathbf{V} + \int_{\mathbf{V}}\{\mathbf{y}(\delta\mathbf{u}) + [\mathbf{Y}(\mathbf{u}_{n+\frac{1}{2}}) + \mathbf{D}_{n+\frac{1}{2}}]\delta\mathbf{w}\}\cdot\{\boldsymbol{\Lambda}^{\mathsf{T}}(\mathbf{R}_{n+\frac{1}{2}})\boldsymbol{\Gamma}^{\mathrm{alg}}_{n+\frac{1}{2}} + \boldsymbol{\Xi}^{\mathsf{T}}(\mathbf{R}_{n+\frac{1}{2}})\cdot\mathbf{L}^{\mathrm{alg}}_{n+\frac{1}{2}}\} \\
&-\int_{\mathbf{V}}\delta\mathbf{u}.\mathbf{f}_{n+\frac{1}{2}}\,\mathrm{d}\mathbf{V} = 0 \\
&(ii) \quad \int_{\mathbf{V}}\{\delta\mathbf{d}\cdot\boldsymbol{\Lambda}^{\mathsf{T}}(\mathbf{R}_{n+\frac{1}{2}})\boldsymbol{\Gamma}^{\mathrm{alg}}_{n+\frac{1}{2}} + \delta\mathbf{d}\cdot\boldsymbol{\Xi}^{\mathsf{T}}(\mathbf{R}_{n+\frac{1}{2}})\mathbf{L}^{\mathrm{alg}}_{n+\frac{1}{2}}\}\,\mathrm{d}\mathbf{V} = 0
\end{aligned}
\tag{15}
$$

which assures energy conservation.

3.2. Energy decaying scheme

Another algorithmic modification is proposed here to control the effect of the high-frequency contribution by developing a time-stepping energy-decaying scheme. In particular, the latter serves as a filter to remove the high-frequency noise, which can not be resolved for a particular finite element mesh on each time step. First, a dissipation term is added to the kinetic energy through the displacement field approximation

$$\mathbf{u}_{n+1} = \frac{\Delta t}{2}[(\dot{\mathbf{u}}_{n+1} + \dot{\mathbf{u}}_n) + \eta_1(\dot{\mathbf{u}}_{n+1} - \dot{\mathbf{u}}_n)] \tag{16}$$

which leads to a new velocity approximation

$$\dot{\mathbf{u}}_{n+1} = \frac{1}{\Delta t(\frac{1}{2} + \eta_1)}\mathbf{u}_{n+1} - \frac{\frac{1}{2} - \eta_1}{\frac{1}{2} + \eta_1}\dot{\mathbf{u}}_n \tag{17}$$

where η_1 is the kinetic energy dissipation coefficient, varying from 0 to 0.5. By taking into account the velocity updates in (17), we can rewrite the kinetic energy increment (11)

$$\Delta \mathbf{T} = \int_{\mathbf{V}} \frac{1}{2}(\dot{\mathbf{u}}_{n+1} + \dot{\mathbf{u}}_n) \cdot \rho(\dot{\mathbf{u}}_{n+1} - \dot{\mathbf{u}}_n)\, \mathrm{d}\mathbf{V} + \eta_1 \int_{\mathbf{V}} (\dot{\mathbf{u}}_{n+1} - \dot{\mathbf{u}}_n) \cdot \rho(\dot{\mathbf{u}}_{n+1} - \dot{\mathbf{u}}_n)\, \mathrm{d}\mathbf{V} = \mathbf{T}_{n+1} - \mathbf{T}_n + \mathbf{D}_T \tag{18}$$

where $\mathbf{D}_T$ is the kinetic energy dissipation part. Similarly, the modified algorithmic constitutive equations contain not only the conservative part as defined in (12) but also dissipating part given as

$$\mathbf{\Gamma}^{\mathrm{alg}}_{n+\frac{1}{2}} = \frac{1}{2}\mathbf{C}\ (\mathbf{e}_{n+1} + \mathbf{e}_n) + \eta_2 \mathbf{C}\ (\mathbf{e}_{n+1} - \mathbf{e}_n);\ \ \mathbf{L}^{\mathrm{alg}}_{n+\frac{1}{2}} = \frac{1}{2}\gamma\ (\boldsymbol{\omega}_{n+1} + \boldsymbol{\omega}_n) + \eta_2 \gamma\ (\boldsymbol{\omega}_{n+1} - \boldsymbol{\omega}_n) \tag{19}$$

where η_2 is the internal energy dissipation coefficient, varying from 0 to 0.5. The corresponding evolution of internal energy in (13) is rewritten as

$$\begin{aligned}
\Delta \Pi_{\mathrm{int}} &= \int_{\mathbf{V}} \{\frac{1}{2}(\mathbf{e}_{n+1} - \mathbf{e}_n) \cdot \mathbf{C}(\mathbf{e}_{n+1} + \mathbf{e}_n) + \eta_2(\mathbf{e}_{n+1} - \mathbf{e}_n) \cdot \mathbf{C}(\mathbf{e}_{n+1} - \mathbf{e}_n)\} \\
&\quad + \{\frac{1}{2}(\boldsymbol{\omega}_{n+1} - \boldsymbol{\omega}_n) \cdot \gamma(\boldsymbol{\omega}_{n+1} + \boldsymbol{\omega}_n) + \eta_2(\boldsymbol{\omega}_{n+1} - \boldsymbol{\omega}_n) \cdot \gamma(\boldsymbol{\omega}_{n+1} - \boldsymbol{\omega}_n)\}\, \mathrm{d}\mathbf{V} \\
&= \int_{\mathbf{V}} \frac{1}{2}\{(\mathbf{e}_{n+1} - \mathbf{e}_n) \cdot \mathbf{C}(\mathbf{e}_{n+1} + \mathbf{e}_n) + (\boldsymbol{\omega}_{n+1} - \boldsymbol{\omega}_n) \cdot \gamma(\boldsymbol{\omega}_{n+1} + \boldsymbol{\omega}_n)\}\, \mathrm{d}\mathbf{V} \\
&\quad + \eta_2 \int_{\mathbf{V}} \{(\mathbf{e}_{n+1} - \mathbf{e}_n) \cdot \mathbf{C}(\mathbf{e}_{n+1} - \mathbf{e}_n) + (\boldsymbol{\omega}_{n+1} - \boldsymbol{\omega}_n) \cdot \gamma(\boldsymbol{\omega}_{n+1} - \boldsymbol{\omega}_n)\}\, \mathrm{d}\mathbf{V} \\
&= \Pi_{\mathrm{int}}|_{n+1} - \Pi_{\mathrm{int}}|_n + \mathbf{D}_\Pi
\end{aligned} \tag{20}$$

where $\mathbf{D}_\Pi$ presents the internal energy dissipation part, having a positive definite quadratic form for positive values of η_2.

By keeping the assumption of an external loading variation as for the energy-conserving case, it is easy to verify that the variational equation in $(9)_{(1)}$ implies

$$\left\{ \begin{matrix} \delta\mathbf{u} \\ \delta\mathbf{w} \end{matrix} \right\} \cdot \mathbf{r}(\mathbf{u}_{n+1}, \mathbf{R}_{n+1}, \mathbf{d}_{n+1}) = 0 \rightarrow \Pi_{n+1} + \mathbf{T}_{n+1} + \mathbf{D}_T + \mathbf{D}_\Pi \succ \Pi_n + \mathbf{T}_n \tag{21}$$

which confirms the energy dissipation for an appropriate choice of dissipation coefficients. For the resolution procedure, we present in details the consistent linearization in appendix B for the conserving time-stepping scheme. It is easy to extend the procedure to the conserving time-stepping scheme.

4. Numerical example

Several numerical examples involving stiff problems are presented in order to illustrate the performance of the proposed time-integration algorithm. All the computations have been performed with a research version of the computer program FEAP, written by Prof. R.L. Taylor at UC Berkeley (e.g., see [8]).

4.1. Simple pendulum

The first example is a pendulum problem adopted from previous work on geometrically exact beams (e.g., see [2]). The pendulum is assumed to be nearly rigid and to have a negligible weight. The finite element model of the pendulum is constructed by 3D enhanced solid elements, where N_{el} is the number of elements. Four concentrated masses are attached to the free end of the pendulum. The latter leaves the rest position by applying an initial horizontal velocity $v = 1.695$ m/s to the attached masses. The gravity force fixed at vertical position does not follow the pendulum swing, then it will perturb the computation of the internal energy via the stress state [12]. For that reason, the contribution of the gravity field is not retained.

This validation test could be classified into the category of stiff problem, since there is a large difference in the associated energy for low swinging modes and high axial vibration modes. As shown in Fig. 1b, the increase of the mesh size is

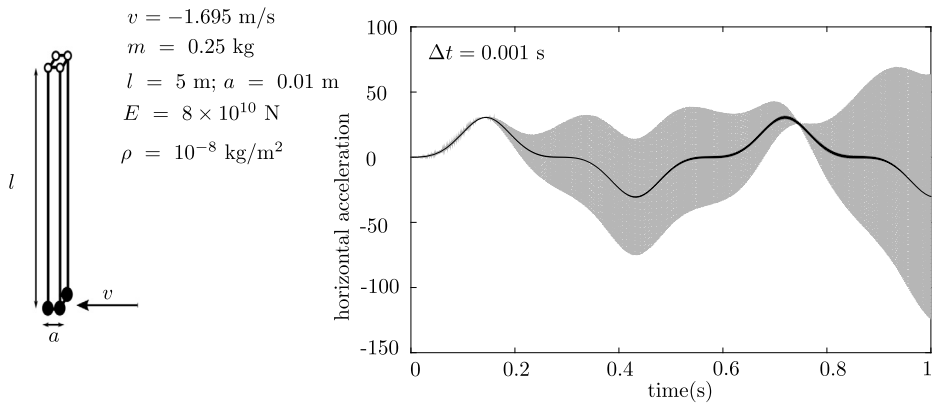

Fig. 1. Simple pendulum test: a) mechanical and geometric properties; b) tip horizontal acceleration obtained by the Newmark scheme and the present energy-conserving scheme.

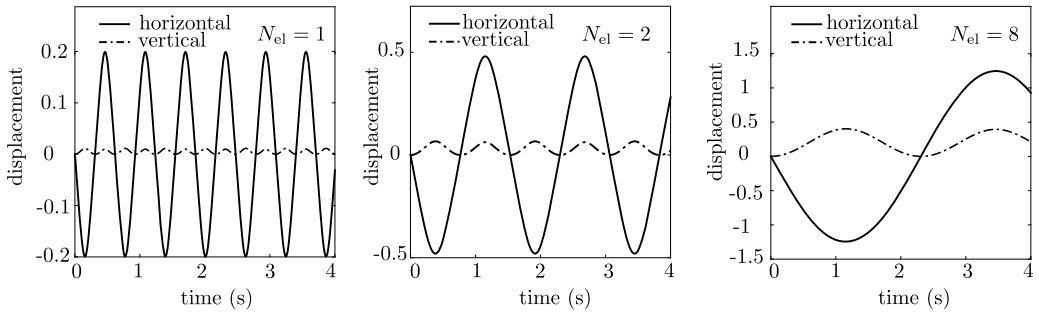

Fig. 2. Simple pendulum test: tip displacement components for different mesh (N_{el} = number of finite elements).

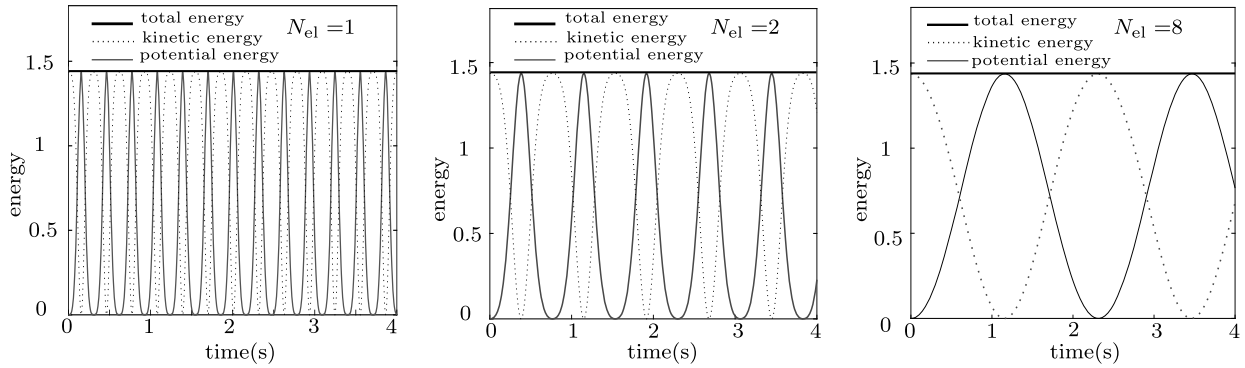

Fig. 3. Simple pendulum test: time history of energy obtained by the energy-conserving scheme (N_{el} = number of finite elements).

accompanied by a change of the low swinging mode. However, the total energy computed by the proposed conserving scheme remains constant (see Fig. 3). We also show in Fig. 2b the high oscillations in the horizontal acceleration obtained by Newmark's scheme against a very smooth time-history acceleration obtained by the proposed energy-conserving scheme. This result is correlated with the constant value of the total energy obtained by the proposed scheme, as shown in Fig. 2a.

4.2. Swing mechanism

This example is adopted from Bauchay et al. [13] as well as from Ibrahimbegovic et al. [2] studied for the beam model. It is used to illustrate the performance of the proposed scheme to conserve energy or to decay it in order to reduce the undesirable contribution of the high-frequency modes. We consider a three-bar swing, composed of a flexible part hinged at its end to almost perfectly two rigid links. All components of this swing mechanism have the same section $A = 5 \times 1$ mm. Four masses are rigidly connected to the flexible part at its mid-span position. The flexible bar is modeled by eight 3D enhanced solid elements. Its selected proprieties are given in Fig. 4a (E_1, ν_1, ρ_1). The rigid links are modeled by one

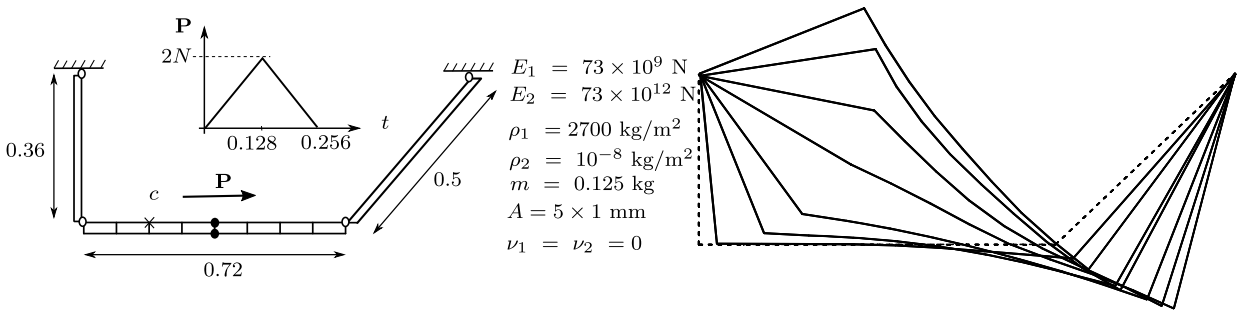

Fig. 4. Three-bar swing: a) initial configuration, mechanical and geometric proprieties and characteristics of loading; b) deformed shape.

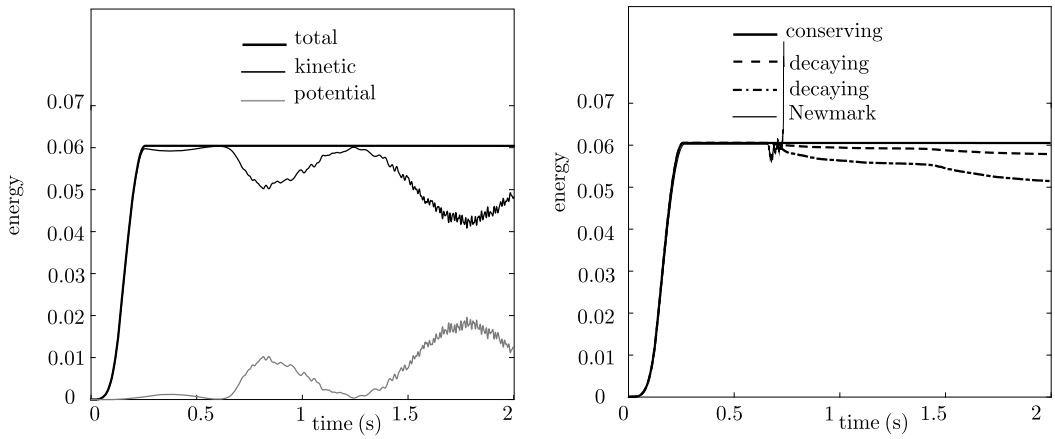

Fig. 5. Three-bar swing: a) time history of the energy obtained by the proposed conserving scheme; b) time history of the energy obtained by different schemes.

element. Its stiffness coefficients are chosen of an order of magnitude greater than those of the flexible part to enforce the stiff problem.

The mechanism is set in motion by a triangular pulse applied horizontally to the masses. The time history of the applied loading is shown in Fig. 4a. The computation is carried out with the time step $\Delta t = 0.0005$, by using the Newmark scheme and the proposed schemes. Some deformed shapes describing the beginning of swing motion are given in Fig. 4b until at approximately $\mathbf{t} = 0.420$ s, obtained by the energy conserving scheme.

As expected, the Newmark scheme is unable to provide a realistic motion and it switches to an infinite level of energy. However, the proposed scheme overcomes the difficulty of stiff problem, ensuring the conservation of the total energy as the plot of time history of energy in 5-a shows. The computation is performed for a significant value of mass regularization, which explains why the total energy is dominated by the value of kinetic energy. In order to illustrate the beneficial effect of mass regularization in controlling Stiff vibrations, we compare the vertical displacement component at a point of flexible part for two extreme cases. In Fig. 6a, we present the high oscillations in the computed displacement obtained for $\alpha = 0.01$ with counterpart a smooth response obtained for $\alpha = 0.1$.

The numerical dissipation is introduced by choosing two different dissipation coefficients. The dissipation is higher from nearly $\mathbf{t} = 1.5$ s, as shown in Fig. 5b, which corresponds to the period of high- oscillation noise. Besides, we notice that the dissipation is greater simply by increasing the dissipation coefficients.

5. Closing remarks

In this paper, we have presented the formulation, numerical analysis and finite element implementation of a time-stepping schemes that ensure energy conservation and energy decay for 3D solid elements with rotational degrees of freedom to analyze geometric nonlinear dynamic problems. The computation instability resulting from the presence of zero masses associated with angular accelerations is well controlled by these schemes, supporting a vastly improved performance in long-term simulations.

The presence of the rotational degree of freedom could proves advantageous in the nonlinear analysis of complex structures combined with the 3D solid model and the geometrically exact beam model, and the energy conserving/decaying schemes ensure the robustness of the computation over very long time intervals.

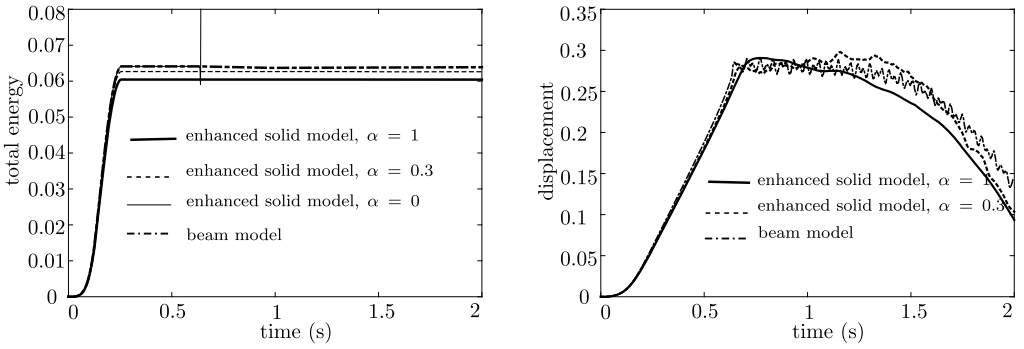

Fig. 6. Three-bar swing: a) comparison of the total energy obtained by the proposed 3D solid model with the total energy obtained by the beam model; b) time history of the vertical displacement component at point C.

It should be emphasized that the energy decaying scheme is naturally constructed as an extension of the energy conserving scheme, with the introduction of numerical dissipation in high modes at each step. In particular, the rotation update remains the same for the energy conserving scheme and the energy decaying one. The modification concerns only the velocity updates and the algorithmic stress resultants. This is quite useful since the two schemes share the same storage pool for the internal variables. Thus, it is very easy to switch from one scheme to another within a single numerical simulation.

The use of the penalty method to introduce the contribution of rotational degrees of freedom plays a part in the elimination of the undesirable affect of infinite frequencies and allows us to produce smoother motion supported by the added masses.

Another computational efficiency gain is the use of the operator split method which allows us to separate the computation of the incompatible mode parameters from the computation of large rotations, and reduces the computation of the these parameters to a single iteration.

Acknowledgements

This work was supported by the French Ministry of Higher Education and Research, as well as the Chair of Mechanics of PICRDIE Funding and the "Institut universitaire" de France (IUF). Their support is gratefully acknowledged.

Appendix A. Compact matrix notation

If we denote by

$$\mathbf{R} = [\mathbf{r}_1, \mathbf{r}_2, \mathbf{r}_3]\,;\;\; [\mathbf{I} + \nabla \mathbf{u}] = [\mathbf{y}_1(\mathbf{u}), \mathbf{y}_2(\mathbf{u}), \mathbf{y}_3(\mathbf{u})]\,;\;\; \mathbf{d}^{\intercal} = \left[\mathbf{d}_1^{\intercal}\mathbf{d}_2^{\intercal}\mathbf{d}_3^{\intercal}\right] \tag{22}$$

the symmetric and skew-symmetric parts of the Biot strain measures $\mathbf{H}$ are mapped as follows

$$\begin{aligned} \mathbf{e}(\mathbf{u}, \mathbf{R}, \mathbf{d}) &= \boldsymbol{\Lambda}(\mathbf{R})(\mathbf{y}(\mathbf{u}) + \mathbf{d}) - \boldsymbol{1} \\ \boldsymbol{\omega}(\mathbf{u}, \mathbf{R}, \mathbf{d}) &= \boldsymbol{\Xi}(\mathbf{R})(\mathbf{y}(\mathbf{u}) + \mathbf{d}) \end{aligned} \tag{23}$$

where

$$\boldsymbol{\Lambda}(\mathbf{R}) = \begin{bmatrix} \mathbf{r}_1^{\intercal} & 0^{\intercal} & 0^{\intercal} \\ 0^{\intercal} & \mathbf{r}_2^{\intercal} & 0^{\intercal} \\ 0^{\intercal} & 0^{\intercal} & \mathbf{r}_3^{\intercal} \\ \mathbf{r}_2^{\intercal} & \mathbf{r}_3^{\intercal} & 0^{\intercal} \\ 0^{\intercal} & \mathbf{r}_3^{\intercal} & \mathbf{r}_1^{\intercal} \\ \mathbf{r}_3^{\intercal} & 0^{\intercal} & \mathbf{r}_2^{\intercal} \end{bmatrix};\; \boldsymbol{\Xi}(\mathbf{R}) = \begin{bmatrix} \mathbf{r}_2^{\intercal} & -\mathbf{r}_1^{\intercal} & 0^{\intercal} \\ 0^{\intercal} & \mathbf{r}_3^{\intercal} & -\mathbf{r}_2^{\intercal} \\ -\mathbf{r}_3^{\intercal} & 0^{\intercal} & \mathbf{r}_1^{\intercal} \end{bmatrix};\; \mathbf{y}(\mathbf{u}) = \begin{pmatrix} \mathbf{y}_1(\mathbf{u}) \\ \mathbf{y}_2(\mathbf{u}) \\ \mathbf{y}_3(\mathbf{u}) \end{pmatrix};\; \boldsymbol{1} = \begin{pmatrix} 1 \\ 1 \\ 1 \\ 0 \\ 0 \\ 0 \end{pmatrix} \tag{24}$$

The variation of strain measures is obtained the directional derivative in the direction of virtual displacement $\delta\mathbf{u}$ and virtual rotation $\delta\mathbf{w}$

$$\begin{aligned} \delta\mathbf{e}(\mathbf{u}, \mathbf{R}, \mathbf{d}) &= \boldsymbol{\Lambda}(\mathbf{R})(\mathbf{y}(\delta\mathbf{u}) + \left[\mathbf{Y}(\mathbf{u}) + \widetilde{\mathbf{D}}\right]\delta\mathbf{w}) \\ \delta\boldsymbol{\omega}(\mathbf{u}, \mathbf{R}, \mathbf{d}) &= \boldsymbol{\Xi}(\mathbf{R})(\mathbf{y}(\delta\mathbf{u}) + \left[\mathbf{Y}(\mathbf{u}) + \widetilde{\mathbf{D}}\right]\delta\mathbf{w}) \end{aligned} \tag{25}$$

Here we use the following tensors:

$$\mathbf{Y}(\mathbf{u}) = \begin{bmatrix} \Upsilon(\mathbf{y}_1(\mathbf{u})) \\ \Upsilon(\mathbf{y}_2(\mathbf{u})) \\ \Upsilon(\mathbf{y}_3(\mathbf{u})) \end{bmatrix};\;\; \widetilde{\mathbf{D}} = \begin{bmatrix} \Upsilon(\mathbf{d}_1) \\ \Upsilon(\mathbf{d}_2) \\ \Upsilon(\mathbf{d}_3) \end{bmatrix};\;\; \Upsilon(\mathbf{v}) = \begin{bmatrix} 0 & v_3 & -v_2 \\ -v_3 & 0 & v_1 \\ v_2 & -v_1 & 0 \end{bmatrix} \tag{26}$$

Appendix B. Consistent linearization of the variational equations: energy conserving algorithm

The operator split methodology is used to separate the computation of the incompatible mode parameters from the computation of large rotation.

(i) $\mathbf{u}$ and $\mathbf{R}$ are fixed

$$[\mathbf{H}]\Delta\widetilde{\boldsymbol{\alpha}}^{e}_{n+1}=\mathbf{h};\ [\mathbf{H}]=\int_{\mathbf{V}}\frac{1}{2}\hat{\mathbf{G}}^{\mathsf{T}}(\boldsymbol{\Lambda}^{\mathsf{T}}(\mathbf{R}_{n+\frac{1}{2}})\mathbf{C}\boldsymbol{\Lambda}(\mathbf{R}_{n+1})+\boldsymbol{\Xi}^{\mathsf{T}}(\mathbf{R}_{n+\frac{1}{2}})\gamma\,\boldsymbol{\Xi}(\mathbf{R}_{n+1}))\,\hat{\mathbf{G}}\ \mathrm{d}\mathbf{V} \tag{27}$$

(ii) $\widetilde{\boldsymbol{\alpha}}$ is computed

$$\begin{aligned}&[\mathbf{M}^{*}]\begin{Bmatrix}\Delta\mathbf{u}^{e}_{n+1}\\ \Delta\mathbf{w}^{e}_{n+1}\end{Bmatrix}+\left([\mathbf{K}^{*}_{m}]+[\mathbf{K}^{*}_{g}]\right)\begin{Bmatrix}\Delta\mathbf{u}^{e}_{n+1}\\ \Delta\mathbf{w}^{e}_{n+1}\end{Bmatrix}+[\mathbf{F}^{*}]\Delta\boldsymbol{\alpha}^{e}_{n+1}=-\mathbf{r}\\ &[\mathbf{F}^{**}]\begin{Bmatrix}\Delta\mathbf{u}^{e}_{n+1}\\ \Delta\mathbf{w}^{e}_{n+1}\end{Bmatrix}+[\mathbf{H}]\,\Delta\boldsymbol{\alpha}^{e}_{n+1}=0\end{aligned} \tag{28}$$

Stiffness and mass matrix:

$$\begin{aligned}&[\mathbf{K}^{*}_{m}]=\int_{\mathbf{V}}\begin{bmatrix}\mathbf{B}^{\mathsf{T}}\\ \hat{\mathbf{Y}}(\mathbf{u}_{n+\frac{1}{2}},\mathbf{d}_{n+\frac{1}{2}})^{\mathsf{T}}\end{bmatrix}\frac{1}{2}\left[\boldsymbol{\Lambda}^{\mathsf{T}}(\mathbf{R}_{n+\frac{1}{2}})\mathbf{C}\boldsymbol{\Lambda}(\mathbf{R}_{n+1})+\boldsymbol{\Xi}^{\mathsf{T}}(\mathbf{R}_{n+\frac{1}{2}})\gamma\,\boldsymbol{\Xi}(\mathbf{R}_{n+1})\right]\left[\mathbf{B},\quad\hat{\mathbf{Y}}(\mathbf{u}_{n+1},\mathbf{d}_{n+1})\right]\mathrm{d}\mathbf{V}\\ &[\mathbf{K}^{*}_{g}]=\int_{\mathbf{V}}\frac{1}{2}\begin{bmatrix}\mathbf{0} & \mathbf{B}^{\mathsf{T}}\mathbf{S}^{\mathsf{T}}_{\boldsymbol{\varrho}}\mathbf{N}\\ \mathbf{N}^{\mathsf{T}}\mathbf{S}_{\boldsymbol{\tau}}\mathbf{B} & \mathbf{N}^{\mathsf{T}}\mathbf{A}_{\boldsymbol{\varrho}}\mathbf{N}\end{bmatrix}\mathrm{d}\mathbf{V};\quad[\mathbf{M}^{*}]=\int_{\mathbf{V}}\begin{bmatrix}\mathbf{N}^{\mathsf{T}}\rho\frac{2}{\Delta t^{2}}\mathbf{N} & 0\\ 0 & \alpha\times\mathbf{N}^{\mathsf{T}}\rho\frac{2}{\Delta t^{2}}\mathbf{N}\end{bmatrix}\mathrm{d}\mathbf{V}\end{aligned} \tag{29}$$

Coupling matrix:

$$\begin{aligned}&[\mathbf{F}^{*}]=\int_{\mathbf{V}}\begin{bmatrix}\mathbf{B}^{\mathsf{T}}\\ \hat{\mathbf{Y}}(\mathbf{u}_{n+\frac{1}{2}},\mathbf{d}_{n+\frac{1}{2}})^{\mathsf{T}}\end{bmatrix}\frac{1}{2}\left[\boldsymbol{\Lambda}^{\mathsf{T}}(\mathbf{R}_{n+\frac{1}{2}})\mathbf{C}\boldsymbol{\Lambda}(\mathbf{R}_{n+1})+\boldsymbol{\Xi}^{\mathsf{T}}(\mathbf{R}_{n+\frac{1}{2}})\gamma\,\boldsymbol{\Xi}(\mathbf{R}_{n+1})\right]\hat{\mathbf{G}}\,\mathrm{d}\mathbf{V}+\int_{\mathbf{V}}\mathbf{N}^{\mathsf{T}}\mathbf{S}^{\mathsf{T}}_{\boldsymbol{\tau}}\hat{\mathbf{G}}\,\mathrm{d}\mathbf{V}\\ &[\mathbf{F}^{**}]=\int_{\mathbf{V}}\hat{\mathbf{G}}^{\mathsf{T}}\frac{1}{2}\left[\boldsymbol{\Lambda}^{\mathsf{T}}(\mathbf{R}_{n+\frac{1}{2}})\mathbf{C}\boldsymbol{\Lambda}(\mathbf{R}_{n+1})+\boldsymbol{\Xi}^{\mathsf{T}}(\mathbf{R}_{n+\frac{1}{2}})\gamma\,\boldsymbol{\Xi}(\mathbf{R}_{n+1})\right]\left[\mathbf{B},\quad\hat{\mathbf{Y}}(\mathbf{u}_{n+1},\mathbf{d}_{n+1})\right]\mathrm{d}\mathbf{V}+\int_{\mathbf{V}}\hat{\mathbf{G}}^{\mathsf{T}}\mathbf{S}^{\mathsf{T}}_{\boldsymbol{\varrho}}\mathbf{N}\,\mathrm{d}\mathbf{V}\end{aligned} \tag{30}$$

Stress resultants matrix:

$$\begin{aligned}&\mathbf{s}_{\boldsymbol{\tau}}=\boldsymbol{\Lambda}^{\mathsf{T}}(\mathbf{R}_{n+\frac{1}{2}})\mathbf{N}_{n+\frac{1}{2}}+\boldsymbol{\Xi}^{\mathsf{T}}(\mathbf{R}_{n+\frac{1}{2}})\mathbf{L}_{n+\frac{1}{2}};\ \ \mathbf{s}_{\boldsymbol{\varrho}}=\boldsymbol{\Lambda}^{\mathsf{T}}(\mathbf{R}_{n+1})\mathbf{N}_{n+\frac{1}{2}}+\boldsymbol{\Xi}^{\mathsf{T}}(\mathbf{R}_{n+1})\mathbf{L}_{n+\frac{1}{2}}\\ &\mathbf{S}=[\mathbf{S}_{1},\mathbf{S}_{2},\mathbf{S}_{3}],\quad\mathbf{S}_{i}\mathbf{b}=\mathbf{s}_{i}\times\mathbf{b},\quad\mathbf{s}^{\mathsf{T}}=[\mathbf{s}^{\mathsf{T}}_{1},\mathbf{s}^{\mathsf{T}}_{2},\mathbf{s}^{\mathsf{T}}_{3}]\\ &\mathbf{A}_{\boldsymbol{\varrho}}=\sum_{i=1}^{3}[\frac{1}{2}\{\mathbf{p}_{\boldsymbol{\varrho},i}\otimes(\mathbf{y}_{i}(\mathbf{u}_{n+\frac{1}{2}})+\mathbf{d}_{n+\frac{1}{2},i})+(\mathbf{y}_{i}(\mathbf{u}_{n+\frac{1}{2}})+\mathbf{d}_{n+\frac{1}{2},i})\otimes\mathbf{p}_{\boldsymbol{\varrho},i}\}-(\mathbf{p}_{\boldsymbol{\varrho},i}\cdot(\mathbf{y}_{i}(\mathbf{u}_{n+\frac{1}{2}})+\mathbf{d}_{n+\frac{1}{2},i}))\mathbf{I}_{3}]\end{aligned} \tag{31}$$

References

[1] J.C. Simo, N. Tarnow, Non-linear dynamics of three dimensional rods: exact energy and momentum conserving algorithms, Int. J. Numer. Methods Eng. 38 (1995) 1431–1473.
[2] A. Ibrahimbegovic, S. Mamouri, Nonlinear dynamics of flexible beams in planar motion: formulation and time-stepping scheme for stiff problems, Comput. Methods Appl. Mech. Eng. 191 (1999) 4241–4258.
[3] A. Ibrahimbegovic, S. Mamouri, Energy conserving/decaying implicit time-stepping scheme for nonlinear dynamics of three-dimensional beams undergoing finite rotations, Comput. Struct. 70 (2002) 1–22.
[4] J.C. Simo, N. Tarnow, The discrete energy-momentum method. Conserving algorithms for nonlinear elastodynamics, Z. Angew. Math. Phys. ZAMP 43 (1992) 757–792.
[5] H.G. Zhong, M.A. Crisfield, An energyconserving corotational procedure for the dynamics of shell structures, Eng. Comput. (1998) 552–576.
[6] A. Ibrahimbegovic, Nonlinear Solid Mechanics: Theoretical Formulations and Finite Element Solution Methods, Springer Science and Business Media, 2009.
[7] C. Gignoux, B. Silvestre-Brac, Solved Problems in Lagrangian and Hamiltonian Mechanics, Springer, Netherlands, 2009.
[8] O.C. Zienkiewicz, R.L. Taylor, The Finite Element Method: Basic Formulation and Linear Problems, vol. I, McGraw-Hill, Maidenhead, England, 1989.
[9] A. Ibrahimbegovic, On the choice of finite rotation parameters, Int. J. Numer. Methods Eng. 149 (1997) 49–71.
[10] J.E. Marsden, Lectures on Mechanics, Cambridge University Press, 1991.
[11] K.V. Spring, Euler parameters and the use of quaternion algebra in the manipulation of finite rotations, Mech. Mach. Theory 21 (1986) 365–373.
[12] A. Ibrahimbegovic, R.L. Taylor, On the role of frame-invariance in structural mechanics models at finite rotations, Comput. Methods Appl. Mech. Eng. 191 (2002) 5159–5176.
[13] G. Damilano, O.A. Bauchau, N.J. Theron, Numerical integration of non-linear elastic multi-body systems, Int. J. Numer. Methods Eng. 38 (1995) 2727–2751.